GeroScience (2022) 44:1621–1639
https://doi.org/10.1007/s11357-022-00564-w

ORIGINAL ARTICLE

Age-related disruption of the proteome and acetylome in mouse hearts is associated with loss of function and attenuated by elamipretide (SS-31) and nicotinamide mononucleotide (NMN) treatment

Jeremy A. Whitson · Richard Johnson · Lu Wang · Theo K. Bammler · Shin-Ichiro Imai · Huiliang Zhang · Jeanne Fredrickson · Elena Latorre-Esteves · Alessandro Bitto · Michael J. MacCoss · Peter S. Rabinovitch

Received: 5 February 2022 / Accepted: 4 April 2022 / Published online: 13 April 2022

Abstract We analyzed the effects of aging on protein abundance and acetylation, as well as the ability of the mitochondrial-targeted drugs elamipretide (SS-31) and nicotinamide mononucleotide (NMN) to reverse aging-associated changes in mouse hearts. Both drugs had a modest effect on restoring the abundance and acetylation of proteins that are altered with age, while also inducing additional changes. Age-related increases in protein acetylation were predominantly in mitochondrial pathways such as mitochondrial dysfunction, oxidative phosphorylation, and TCA cycle signaling. We further assessed how these age-related changes associated with diastolic function (Ea/Aa) and systolic function (fractional shortening under higher workload) measurements from echocardiography. These results identify a subset of protein abundance and acetylation changes in muscle, mitochondrial, and structural proteins that appear to be essential in regulating diastolic function in old hearts.

Keywords Aging · Mitochondria · Heart · Elamipretide · SS-31 · NMN · Proteomics · Acetylomics

Supplementary Information The online version contains supplementary material available at https://doi.org/10.1007/s11357-022-00564-w.

J. A. Whitson
Department of Biology, Davidson College, 405 N Main St, Davidson, NC 28035, USA

R. Johnson
Department of Genome Sciences, University of Washington, 3720 15th Street NE, Seattle, WA 98195, USA

L. Wang · T. K. Bammler
Department of Environmental & Occupational Health Sciences, University of Washington, 4225 Roosevelt Way NE, Seattle, WA 98105, USA

S.-I. Imai
Department of Developmental Biology, Washington University School of Medicine, 660 South Euclid Avenue, St. Louis, MO 63110, USA

H. Zhang
Department of Pharmacology and Toxicology, University of Arkansas for Medical Sciences, 4301 W Markham St, Little Rock, AR 72205, USA

J. Fredrickson · E. Latorre-Esteves · A. Bitto · M. J. MacCoss · P. S. Rabinovitch (✉)
Department of Pathology, University of Washington, 1959 NE Pacific St, Seattle, WA 98195, USA
e-mail: petersr@u.washington.edu

Introduction

Alteration of the proteome is an established correlate of aging at the cellular level and includes changes in protein abundance due to gene expression changes and a loss of proteostasis, and changes in post-translational modifications (PTMs) of proteins [10, 13, 16]. This applies to the heart, which has demonstrated age-related changes in protein abundance [4, 11] and PTMs [2, 19] that appear to contribute to cardiac dysfunction [3].

Among the most common PTMs are non-enzymatic acetylation of lysine residues, occurring primarily in mitochondrial proteins due to the high levels of acetyl-CoA present [1]. One recent study reported that acetylation of both electron transport chain proteins and the total heart proteome increases significantly with age [20]. While accumulation of such damaging acetylation is expected with age, the aging process may also lead to the loss of desirable acetylation of specific residues across the proteome, which normally serve roles in signaling and cellular regulation [13].

Rewinding the proteome to a more youthful state has been proposed as a way to repair functional deficits that occur with age. Since mitochondria show substantial changes in acetylation with age, alteration of the acetylation state could be one mechanism by which mitochondrial-targeted anti-aging drugs carry out their function. Elamipretide (originally known as SS-31 and subsequently referred to as ELAM) and nicotinamide mononucleotide (NMN) are two mitochondrial-targeted drugs that we have previously demonstrated to effectively restore cardiac function in old mice, with elamipretide primarily enhancing diastolic function and NMN enhancing systolic function under higher workload [18]. To test and compare the effects of the drugs, old mice (24 months of age at the start of treatment) were randomized to control, elamipretide, and NMN treatment groups and treated for 8 weeks, and further compared to young (5–6 months of age) mice. After treatment, heart tissue was collected for analysis of protein abundance and acetylation. To further determine how proteomic changes link to functional changes induced by these drugs, an association analysis was performed to compare levels of protein abundance and acetylation with measures of diastolic and systolic function.

Results

Elamipretide and NMN treatments attenuate age-related changes in essential pathways while inducing additional changes in others

Assessment of protein abundance was performed by data-independent acquisition (DIA) shotgun proteomics. Principal component analysis (PCA) of the resulting data showed that young and old clustered apart along PC1 and PC2 (Fig. 1A). The old NMN and elamipretide-treated samples did not separate from the old control along PC1 but did appear to show partial separation from old control, and movement towards young samples, along PC2. In total, 269 proteins showed significant (false discovery rate [FDR] < 0.1) abundance changes with age in control mice, while neither elamipretide nor NMN showed any effects on individual protein abundances that reached an FDR < 0.1 threshold of change (Fig. 1B). The 50 changes with the lowest *P*-values in the young vs old control comparison are shown in Table 1 and the full set of results can be found in Appendix 1. Notably, multiple electron transport chain–associated genes can be found in Table 1, including cytochrome C oxidase subunits and those involved in the biosynthesis of coenzyme Q.

General trends in canonical pathways based on protein abundance changes that reached unadjusted $P < 0.05$ were analyzed using Ingenuity Pathway Analysis software (IPA; QIAGEN, Hilden, Germany). IPA generates a, "activation z-score," up- and downregulation, and also to predict the activation state (either activated or inhibited) of a putative regulator [5]. This analysis showed significant age-related shifts in pathways including mitochondrial dysfunction, oxidative phosphorylation, and sirtuin signaling (Fig. 1C), indicating that mitochondrial protein abundance was particularly affected by aging. Calcium signaling also showed significant alteration, which included essential cardiac proteins like troponin and tropomyosin subunits. Notably, the oxidative phosphorylation pathway (which consists of an overlapping subset of proteins from the mitochondrial dysfunction pathway) was significantly activated in young, old + elamipretide, and old + NMN hearts relative to old control (Fig. 1D). Generally, elamipretide and NMN resulted in the same pathways being activated and inactivated as were seen in the young to

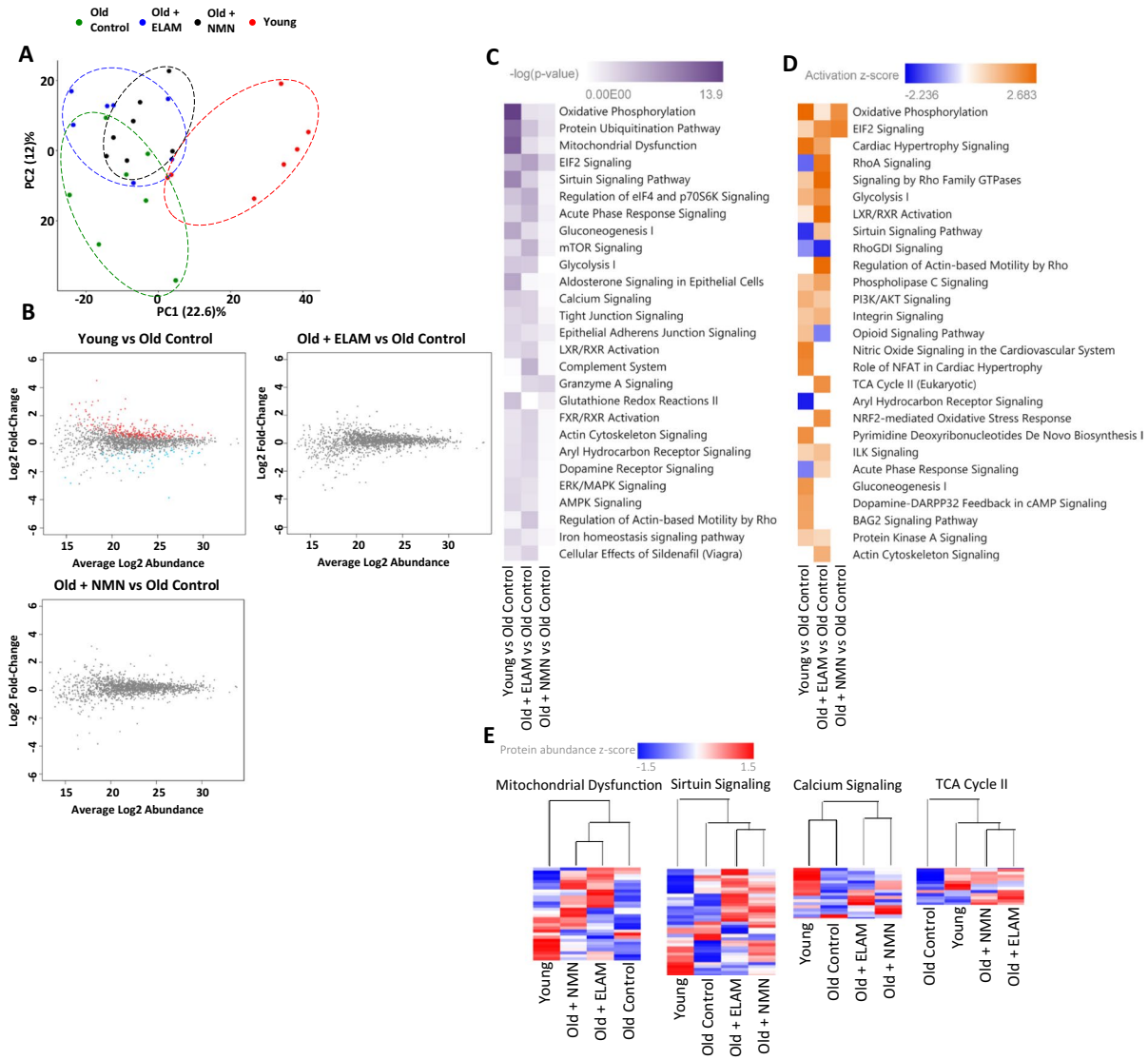

Fig. 1 Analysis of protein abundance in mouse hearts. **A** Principal component analysis of proteomic data. Each dot represents one sample. Circled regions identify the location of all samples in one group. **B** Mean difference plots of protein in abundance in young, old + elamipretide, and old + NMN compared to old control. Each dot represents one protein. Proteins with significantly (FDR < 0.1) higher abundance in the comparison are colored red, while those with significantly lower abundance are colored blue. **C** *P*-value heatmap of protein abundance changes in canonical pathways based on all changes with an unadjusted $P < 0.05$. Top 25 pathways, ranked by *P*-value, are shown. **D** Activation *Z*-score heatmap of protein abundance changes in canonical pathways based on all changes with an unadjusted $P < 0.05$. Top 25 pathways, ranked by *Z*-score, are shown. **E** Row-normalized *Z*-score heatmaps of significant (unadjusted $P < 0.05$) protein abundance differences in selected pathways

old control comparison, but with some exceptions. While significantly impacted in each group, sirtuin signaling pathway protein abundance was inactivated in young, activated in old + elamipretide, and did not show a clear directionality in old + NMN relative to old control. Visualizing the effects on individual pathways also shows that clustering was not uniform across pathways (Fig. 1E). In these heatmaps, we see that elamipretide and NMN treatment seemed to shift old hearts further away from the young state, whereas

Table 1 50 significant age-related protein abundance changes in mouse hearts. Bold numbers indicate significance (FDR < 0.1). Ordered by lowest P-value in Young vs Old Control comparison. Full results can be found in Appendix 1

Protein	Fold Change Relative to Old Control		
	Young	Old + ELAM	Old + NMN
MFGE8	**0.26**	1.15	0.95
PLIN5	**3.36**	0.62	0.79
HSPB1	**1.55**	1.21	1.00
MLYCD	**2.35**	1.18	1.59
Cox5b	**1.69**	1.03	1.16
STIP1	**1.51**	1.02	1.05
COX5A	**1.51**	1.06	1.18
TNNC1	**1.91**	1.05	1.17
PFDN5	**1.87**	0.99	1.06
PLIN3	**2.49**	0.83	0.92
TOM1	**1.75**	0.90	1.06
AK3	**1.73**	0.99	0.97
COA7	**1.94**	1.05	1.02
NDRG2	**2.40**	1.01	1.10
Cox8b	**22.74**	0.61	4.60
SERPINH1	**2.74**	1.48	1.66
COQ9	**1.95**	1.10	1.14
CKM	**1.54**	0.85	0.91
UCHL3	**2.09**	1.06	1.36
EEF1D	**1.74**	1.26	1.13
HP	**0.07**	1.25	0.54
PFDN6	**2.56**	1.13	1.43
AK1	**1.42**	1.00	1.02
PPM1B	**2.05**	1.20	1.30
EIF3J	**2.07**	0.95	1.26
Mt2	**0.24**	1.83	1.12
NDUFS8	**1.69**	0.87	0.88
HPRT1	**0.31**	1.28	1.36
RBBP4	**2.67**	1.40	1.62
NSFL1C	**1.46**	1.12	1.08
RBM8A	**3.28**	1.38	1.92
TACO1	**1.79**	1.16	1.25
GLRX3	**1.60**	1.24	1.03
PDHX	**1.38**	1.03	1.01
PDIA6	**1.86**	1.08	0.87
DDT	**9.24**	1.39	0.97
GRSF1	**7.94**	0.53	2.70
COQ3	**2.22**	1.53	1.52
AK4	**2.39**	1.04	1.05
PTGDS	**0.29**	1.23	1.05
FBLN5	**2.67**	1.78	1.13
PPA2	**1.62**	0.90	1.13
HSPB2	**1.56**	1.26	1.30
DGLUCY	**1.58**	1.11	1.25
CBX1	**1.80**	1.00	1.34
CAPRIN1	**1.57**	1.21	1.40
RILP	**3.79**	1.30	1.89
NDUFV2	**1.30**	1.00	1.11
HSPA9	**1.55**	1.05	0.96
COQ8A	**1.54**	0.74	0.89

they had a largely restorative effect on TCA cycle proteins.

Aging and drug treatments impact acetylation of essential heart and mitochondrial pathways

From the same preparation as the protein abundance analysis described above, a portion of each sample was subjected to pulldown on acetyl-lysine antibody–conjugated beads for enrichment of acetylated peptides. The acetyl-lysine-enriched samples were then analyzed by the same DIA proteomics technique as described above. Principal component analysis of the acetylated peptides did not show any clear separation of the groups along PC1 but did show segregation of young and old along PC2 (Fig. 2A). Elamipretide treatment appeared to result in further movement away from young, primarily along PC2. A total of 501 acetylation sites showed significant modification with age (FDR < 0.1) (Fig. 2B). No differences between the old control and old + elamipretide group reached the FDR < 0.1 threshold of significance. However, the old + NMN group, relative to old control, did show significantly increased acetylation in peptides mapping to ATP5J (ATP synthase–coupling factor 6), DECR (2,4-dienoyl-CoA reductase), ACO13 (acyl-coenzyme A thioesterase 13), ATPO (ATP synthase subunit O), RS30 (40S ribosomal protein S30), and ECHA (trifunctional enzyme subunit alpha). Interestingly, most of these proteins play an essential role in mitochondrial energetics. Peptides from ATPO and DECR also showed significantly greater acetylation in young mouse hearts compared to old control, though only DECR also showed significantly increased acetylation at the exact same

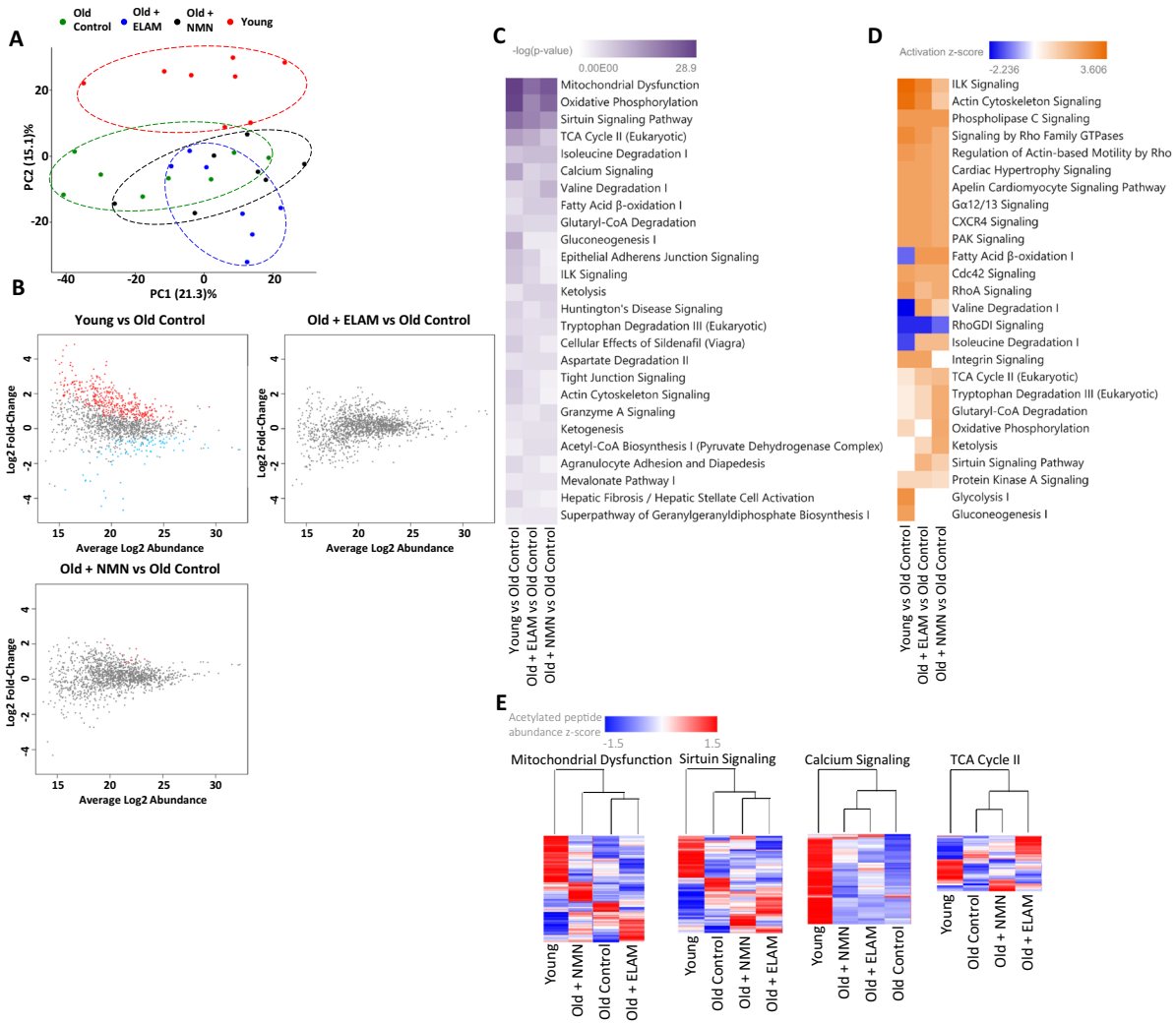

Fig. 2 Analysis of acetylated peptides in mouse hearts. **A** Principal component analysis of acetylomic data. Each dot represents one sample. Circled regions identify the location of all samples in one group. **B** Mean difference plots of acetylated peptide abundance in young, old + elamipretide, and old + NMN compared to old control. Each dot represents one acetylated peptide. Peptides with significantly (FDR < 0.1) higher abundance in the comparison are colored red, while those with significantly lower abundance are colored blue. **C** *P*-value heatmap of peptide acetylation changes in canonical pathways based on all changes with an unadjusted $P < 0.05$. Top 25 pathways, ranked by *P*-value, are shown. **D** Activation *Z*-score heatmap of acetylated peptide changes in canonical pathways based on all changes with an unadjusted $P < 0.05$. Top 25 pathways, ranked by *Z*-score, are shown. **E** Row-normalized *Z*-score heatmaps of significant ($P < 0.05$) peptide acetylation differences in selected pathways

residues when comparing old NMN mice to old control mice. The 50 changes with the lowest *P*-values in the young vs old control comparison are shown in Table 2 and the full set of results can be found in Appendix 2.

One potential concern with this approach is that apparent differences in acetylated peptides might actually be due to changes only in the total abundance of the protein, with a preserved proportion of acetylation. Comparison of the results in Appendices 1 and 2 reveals that 96% of the acetylated peptides map to proteins that were detected in our abundance measurement but only 8% of these showed a significant (FDR < 0.1) change in abundance (Supplemental Fig. 1). Thus, while we cannot definitively say for every single acetylated peptide

Table 2 50 significant age-related acetylation changes in mouse hearts. Bold numbers indicate significance (FDR < 0.1). Ordered by P-value in Young vs Old Control Comparison. Full results can be found in Appendix 2

Peptide	Maps to Proteins	Fold Change Relative to Old Control		
		Young	Old + ELAM	Old + NMN
ASFTK[+42]SLQGIR	*sp|Q02788|CO6A2_MOUSE:tr|D3Z7D5|D3Z7D5_MOUSE*	**0.06**	0.98	0.58
LVEK[+42]FLEEAK	*sp|P07758|A1AT1_MOUSE:sp|P22599|A1AT2_MOUSE:sp|Q00896|A1AT3_MOUSE:sp|Q00897|A1AT4_MOUSE:sp|Q00898|A1AT5_MOUSE:tr|A0A0A0MQA3|A0A0A0MQA3_MOUSE:tr|A0A0R4J0X5|A0A0R4J0X5_MOUSE*	**2.22**	1.31	1.14
DLSYK[+42]DR	*sp|O70433|FHL2_MOUSE*	**0.16**	1.19	1.19
MEIQEIQLK[+42]EAK	*sp|P58771|TPM1_MOUSE:tr|B7ZNL3|B7ZNL3_MOUSE:tr|E9Q448|E9Q448_MOUSE:tr|E9Q450|E9Q450_MOUSE:tr|E9Q452|E9Q452_MOUSE:tr|E9Q453|E9Q453_MOUSE:tr|E9Q454|E9Q454_MOUSE:tr|E9Q455|E9Q455_MOUSE:tr|E9Q456|E9Q456_MOUSE:tr|F8WID5|F8WID5_MOUSE:tr|G5E8R0|G5E8R0_MOUSE:tr|G5E8R1|G5E8R1_MOUSE:tr|G5E8R2|G5E8R2_MOUSE:sp|P58771-2|TPM1_MOUSE:tr|Q8BP43|Q8BP43_MOUSE:tr|Q8BSH3|Q8BSH3_MOUSE*	**2.60**	1.15	1.81
VFDK[+42]EGNGTVMGAEIR	*sp|Q60605|MYL6_MOUSE:sp|Q60605-2|MYL6_MOUSE*	**22.73**	1.84	1.46
HQIQSYTC[+57]EIDALK[+42]GTNDSLMR	*sp|P31001|DESM_MOUSE*	**3.29**	1.44	1.76
HQGVMVGMGQK[+42]DSYVGDEAQSK	*sp|P60710|ACTB_MOUSE:sp|P62737|ACTA_MOUSE:sp|P63260|ACTG_MOUSE:sp|P63268|ACTH_MOUSE:sp|P68033|ACTC_MOUSE:sp|P68134|ACTS_MOUSE:tr|D3YZY0|D3YZY0_MOUSE:tr|D3Z2K3|D3Z2K3_MOUSE:tr|E9Q5F4|E9Q5F4_MOUSE:tr|E9Q606|E9Q606_MOUSE:tr|G3UYG0|G3UYG0_MOUSE:tr|G3UZ07|G3UZ07_MOUSE*	**4.62**	1.64	2.46

Table 2 (continued)

Peptide	Maps to Proteins	Fold Change Relative to Old Control		
		Young	Old + ELAM	Old + NMN
LTMFGEK[+42]LK	*sp|P51667|MLRV_MOUSE:sp|Q62082|MYL10_MOUSE:tr|A0A0G2JDZ4|A0A0G2JDZ4_MOUSE:tr|A0A0G2JE15|A0A0G2JE15_MOUSE:tr|D3YUI7|D3YUI7_MOUSE:tr|D3YW14|D3YW14_MOUSE:tr|D3Z0I3|D3Z0I3_MOUSE:tr|E9Q8Y0|E9Q8Y0_MOUSE:tr|E9QNY3|E9QNY3_MOUSE:sp|Q62082-2|MYL10_MOUSE:sp|Q62082-3|MYL10_MOUSE:sp|P97457|MLRS_MOUSE:tr|A0A0U1RP93|A0A0U1RP93_MOUSE:tr|A0A0U1RQ36|A0A0U1RQ36_MOUSE*	**18.04**	1.60	0.79
VVK[+42]QASEGPLK	*sp|P16858|G3P_MOUSE:tr|S4R1W1|S4R1W1_MOUSE:tr|A0A0A0MQF6|A0A0A0MQF6_MOUSE:tr|S4R257|S4R257_MOUSE*	**3.43**	1.45	2.14
VYINLDK[+42]ETK	*sp|P52503|NDUS6_MOUSE*	**3.43**	1.45	2.14
VYINLDKETK[+42]	*sp|P52503|NDUS6_MOUSE*	**4.47**	1.68	2.33
EITALAPSTMKIK[+42]	*sp|P60710|ACTB_MOUSE:sp|P62737|ACTA_MOUSE:sp|P63260|ACTG_MOUSE:sp|P63268|ACTH_MOUSE:sp|P68033|ACTC_MOUSE:sp|P68134|ACTS_MOUSE:tr|B1ATY1|B1ATY1_MOUSE:tr|E9Q1F2|E9Q1F2_MOUSE:tr|F8WGM8|F8WGM8_MOUSE*	**0.24**	1.19	0.60
TVTNNLK[+42]SLEAQAEK	*sp|P58771|TPM1_MOUSE:tr|B7ZNL3|B7ZNL3_MOUSE:tr|E9Q452|E9Q452_MOUSE:tr|E9Q454|E9Q454_MOUSE:tr|E9Q455|E9Q455_MOUSE:tr|F8WID5|F8WID5_MOUSE:tr|G5E8R0|G5E8R0_MOUSE:tr|G5E8R1|G5E8R1_MOUSE:sp|P58771-2|TPM1_MOUSE:tr|Q8BSH3|Q8BSH3_MOUSE*	**27.23**	1.21	1.90
VYFAEK[+42]VTSLGK	*sp|Q9DCT8|CRIP2_MOUSE:tr|A0A0G2JF37|A0A0G2JF37_MOUSE*	**7.14**	1.47	2.78
AFFK[+42]GAWSNVLR	*sp|P48962|ADT1_MOUSE:sp|P51881|ADT2_MOUSE*	**28.60**	1.39	2.93
SFHK[+42]TC[+57]FHC[+57]	*sp|P50462|CSRP3_MOUSE*	**12.39**	3.39	4.87
VASNLNLKPGEC[+57]LK[+42]VR	*sp|P16045|LEG1_MOUSE*	**3.41**	1.37	1.95
GTQC[+57]EK[+42]IVQK	*sp|Q9R0Y5|KAD1_MOUSE:tr|A0A0A6YXW8|A0A0A6YXW8_MOUSE:sp|Q9R0Y5-2|KAD1_MOUSE:tr|Z4YN97|Z4YN97_MOUSE*	**2.25**	1.25	1.60

Table 2 (continued)

Peptide	Maps to Proteins	Fold Change Relative to Old Control		
		Young	Old + ELAM	Old + NMN
AITATQK[+42]TVDGPSGK	*tr|D3YYI5|D3YYI5_MOUSE:sp|P16858|G3P_MOUSE:tr|S4R1W1|S4R1W1_MOUSE:tr|V9GX06|V9GX06_MOUSE:tr|V9GXA7|V9GXA7_MOUSE:tr|A0A0A0MQF6|A0A0A0MQF6_MOUSE:tr|S4R257|S4R257_MOUSE*	**4.38**	2.02	2.47
NVLINK[+42]DIR	*sp|P14211|CALR_MOUSE*	**13.00**	1.08	0.89
VESQLK[+42]ILIRPLYSNPPLNGAR	*sp|P05202|AATM_MOUSE*	**2.27**	1.46	1.26
QWHNDC[+57]FNC[+57]KK[+42]	*sp|O70433|FHL2_MOUSE*	**3.34**	1.23	1.88
C[+57]GSSLVDK[+42]PFAAK	*sp|O70433|FHL2_MOUSE*	**0.06**	0.81	0.86
QWHNDC[+57]FNC[+57]K[+42]K	*sp|O70433|FHL2_MOUSE*	**9.50**	1.70	0.89
EC[+57]FVC[+57]TAC[+57]K[+42]K	*sp|O70433|FHL2_MOUSE*	**2.84**	0.74	0.96
EC[+57]FVC[+57]TAC[+57]KK[+42]	*sp|O70433|FHL2_MOUSE*	**4.27**	1.19	1.11
VINDFVEKGTQGK[+42]	*sp|P07758|A1AT1_MOUSE:sp|P22599|A1AT2_MOUSE:sp|Q00896|A1AT3_MOUSE:sp|Q00897|A1AT4_MOUSE:sp|Q00898|A1AT5_MOUSE:tr|A0A0A0MQA3|A0A0A0MQA3_MOUSE:tr|A0A0R4J0X5|A0A0R4J0X5_MOUSE*	**2.65**	1.25	1.26
C[+57]VSK[+42]YLDIHER	*sp|P62073|TIM10_MOUSE*	**2.65**	1.25	1.26
VINDFVEK[+42]GTQGK	*sp|P07758|A1AT1_MOUSE:sp|P22599|A1AT2_MOUSE:sp|Q00896|A1AT3_MOUSE:sp|Q00897|A1AT4_MOUSE:sp|Q00898|A1AT5_MOUSE:tr|A0A0A0MQA3|A0A0A0MQA3_MOUSE:tr|A0A0R4J0X5|A0A0R4J0X5_MOUSE*	**3.90**	1.04	1.27
K[+42]FLMEC[+57]R	*sp|Q60876|4EBP1_MOUSE*	**3.36**	1.18	1.34
MQMLK[+42]LDKENAIDR	*sp|P58774|TPM2_MOUSE:tr|A2AIM4|A2AIM4_MOUSE:tr|A2AIM5|A2AIM5_MOUSE:sp|P58774-2|TPM2_MOUSE*	**2.38**	1.44	1.35

Table 2 (continued)

Peptide	Maps to Proteins	Fold Change Relative to Old Control		
		Young	Old + ELAM	Old + NMN
MQMLK[+42]LDK	*sp|P21107|TPM3_MOUSE:sp|P58771|TPM1_MOUSE:sp|P58774|TPM2_MOUSE:tr|A0A0R4J1P2|A0A0R4J1P2_MOUSE:tr|A2AIM4|A2AIM4_MOUSE:tr|A2AIM5|A2AIM5_MOUSE:tr|B7ZNL3|B7ZNL3_MOUSE:tr|E9Q448|E9Q448_MOUSE:tr|E9Q450|E9Q450_MOUSE:tr|E9Q452|E9Q452_MOUSE:tr|E9Q454|E9Q454_MOUSE:tr|E9Q5J9|E9Q5J9_MOUSE:tr|F8WID5|F8WID5_MOUSE:sp|P58771-2|TPM1_MOUSE:sp|P58774-2|TPM2_MOUSE:tr|Q8BP43|Q8BP43_MOUSE:tr|Q8BSH3|Q8BSH3_MOUSE:tr|S4R2U0|S4R2U0_MOUSE*	**2.33**	1.22	1.38
ENLNK[+42]LMTNLK	*sp|Q02566|MYH6_MOUSE:sp|Q5SX39|MYH4_MOUSE*	**0.04**	1.29	1.39
C[+57]AADLGLK[+42]R	*sp|P70349|HINT1_MOUSE*	**2.02**	1.16	1.41
FGESEK[+42]C[+57]PR	*sp|P50462|CSRP3_MOUSE*	**2.38**	1.24	1.42
ENQNFC[+57]VPC[+57]YEK[+42]QYALQC[+57]VQC[+57]K	*sp|O70433|FHL2_MOUSE*	**2.03**	1.33	1.55
LAAEK[+42]GIDLTQVK	*sp|Q8BMF4|ODP2_MOUSE*	**3.36**	1.12	1.78
LSC[+57]LYGK[+42]IYQR	*sp|Q71RI9|KAT3_MOUSE:tr|A0A0G2JGE1|A0A0G2JGE1_MOUSE:sp|Q71RI9-2|KAT3_MOUSE*	**2.59**	1.36	1.79
VFVSPLAK[+42]K	*sp|Q8BMF4|ODP2_MOUSE*	**13.89**	3.18	1.98
ALDSTTVAAHESEIYC[+57]K[+42]VC[+57]YGR	*sp|P50462|CSRP3_MOUSE*	**3.68**	2.07	2.72
LKPGEC[+57]LK[+42]VR	*sp|P16045|LEG1_MOUSE*	**7.96**	2.02	2.91
VFVSPLAKK[+42]	*sp|Q8BMF4|ODP2_MOUSE*	**6.69**	3.27	2.06
DFGSFEK[+42]FKEK	*sp|P09671|SODM_MOUSE*	**2.04**	1.22	1.55
NYK[+42]TAPFDSR	*sp|P56391|CX6B1_MOUSE*	**2.23**	1.25	1.88
HPK[+42]FEEILTR	*sp|P07310|KCRM_MOUSE:sp|KCRM_HUMAN|*	**6.57**	2.75	4.08
MM[+16]DFETFLPMLQHISKNK[+42]	*sp|P09542|MYL3_MOUSE:tr|A0A0G2JDM3|A0A0G2JDM3_MOUSE:tr|A0A0G2JDW2|A0A0G2JDW2_MOUSE*	**8.14**	1.19	3.35
GVWK[+42]GLFAR	*sp|Q8VEM8|MPCP_MOUSE:tr|G5E902|G5E902_MOUSE*	**0.27**	1.10	0.71
TGEGFYKYK[+42]	*sp|Q61425|HCDH_MOUSE*	**3.27**	1.25	1.88
HGC[+57]TVLTALGTILK[+42]K	*sp|P04247|MYG_MOUSE*	**3.12**	1.17	1.65
VAQLC[+57]DFNPK[+42]SSK	*sp|Q6IRU5|CLCB_MOUSE:sp|Q6IRU5-2|CLCB_MOUSE*	**4.06**	0.93	1.94

that the results were not influenced by changes in protein abundance, it is clear that the major trends in the acetylation data are not driven by shifts in protein abundance.

We again performed an analysis of canonical pathways in the acetylation data based on all changes with an unadjusted $P < 0.05$ using IPA (Fig. 2C and D). Again, essential mitochondrial and heart pathways, such as oxidative phosphorylation, TCA cycle, and calcium signaling, were significantly impacted. In most cases, elamipretide and NMN had a similar impact on pathway activation (i.e., whether acetylation of the pathway increased or decreased overall) as to when young was compared to old control. The only exceptions to this were fatty acid β-oxidation, valine degradation, and isoleucine degradation, where the young vs old control comparison showed deactivation of the pathway, while the comparison of treated vs untreated old mice showed activation of the pathway. Heatmaps of individual pathways show that the clustering of the groups varies depending on the pathway in question (Fig. 2E). It is clear from this data that the old control and old + NMN groups clustered more closely with the young within these pathways than old + elamipretide did, consistent with the PCA data.

NMN treatment is expected to increase the activity of the NAD^+-dependent deacetylase family of sirtuin proteins, the likely mechanism for reversing any age-related hyperacetylation, and sirtuin signaling appeared repeatedly as an impacted pathway; therefore, a general assay for sirtuin activity was performed on mouse heart tissue (Supplemental Fig. 2). Since mitochondrial proteins were particularly impacted by age-related acetylation changes, which were attenuated by NMN treatment, and because Sirt3 is especially important in mitochondria, tissues from young and old Sirt3 knockout mice were included in this assay. No significant differences in total sirtuin activity were detected between any of the groups tested. However, because no differences were detected in either the young or old Sirt3 knockout hearts, we conclude that Sirt3 activity is too small a proportion of total heart sirtuin activity to be detected in this assay, indicating that modulation of Sirt3 activity by aging, elamipretide, and/or NMN remains a possibility, even if activity of more abundant sirtuin isoforms, such as Sirt1, is not affected by these treatments.

Heart protein abundance and peptide acetylation differences associate with functional differences

In an effort to gain deeper insight into how proteomic differences may affect heart function, we developed a statistical model to determine which protein abundance and peptide acetylation changes in the old control mice are associated with measures of heart health obtained from the same individual mice by echocardiography. We examined the Ea/Aa ratio, a measure of diastolic function related to the peak velocity of ventricular filling, and fractional shortening under higher work conditions induced by the drug dobutamine as a measure of systolic function. We previously observed that both of these measures show a significant decrease with age and that elamipretide can partially restore Ea/Aa while NMN can fully restore high workload fractional shortening, but not vice versa [18]. Individual examples of this association analysis can be found in Fig. 3A–C.

We identified 28 proteins whose levels were significantly (FDR < 0.1) associated with Ea/Aa, all of which were in old elamipretide-treated hearts, with the exception of hypoxanthine phosphoribosyltransferase 1 (HPRT) (Table 3). HPRT showed a strong negative association with Ea/Aa, meaning that lower levels of the protein are associated with higher Ea/Aa measurements, and vice versa, in young mouse hearts. Proteins that associated with Ea/Aa in old elamipretide-treated hearts included those with a known role in cardiac function and mitochondrial health, such as troponin T (TNNT2), paladin (PALLD), and SRA stem-loop-interacting RNA-binding protein, mitochondrial (SLIRP) as well as proteins without a characterized role in heart tissue such as transforming acidic coiled-coil-containing protein 2 (TACC2). No proteins significantly (FDR < 0.1) associated with high work fractional shortening in any of the groups. The full set of protein abundance association results for all groups can be found in Appendix 1.

A total of 14 acetylation sites showed significant (FDR < 0.1) association with Ea/Aa (Tables 4 and 5). This includes superoxide dismutase [Mn/Fe]^2 (SODM) in young hearts, beta-globin (Hbb-bs) in old elamipretide-treated hearts, and several sites in old control hearts, including multiple locations on myosin chains. In all cases, the association was strongly negative, indicating that greater acetylation at these sites correlated with decreased

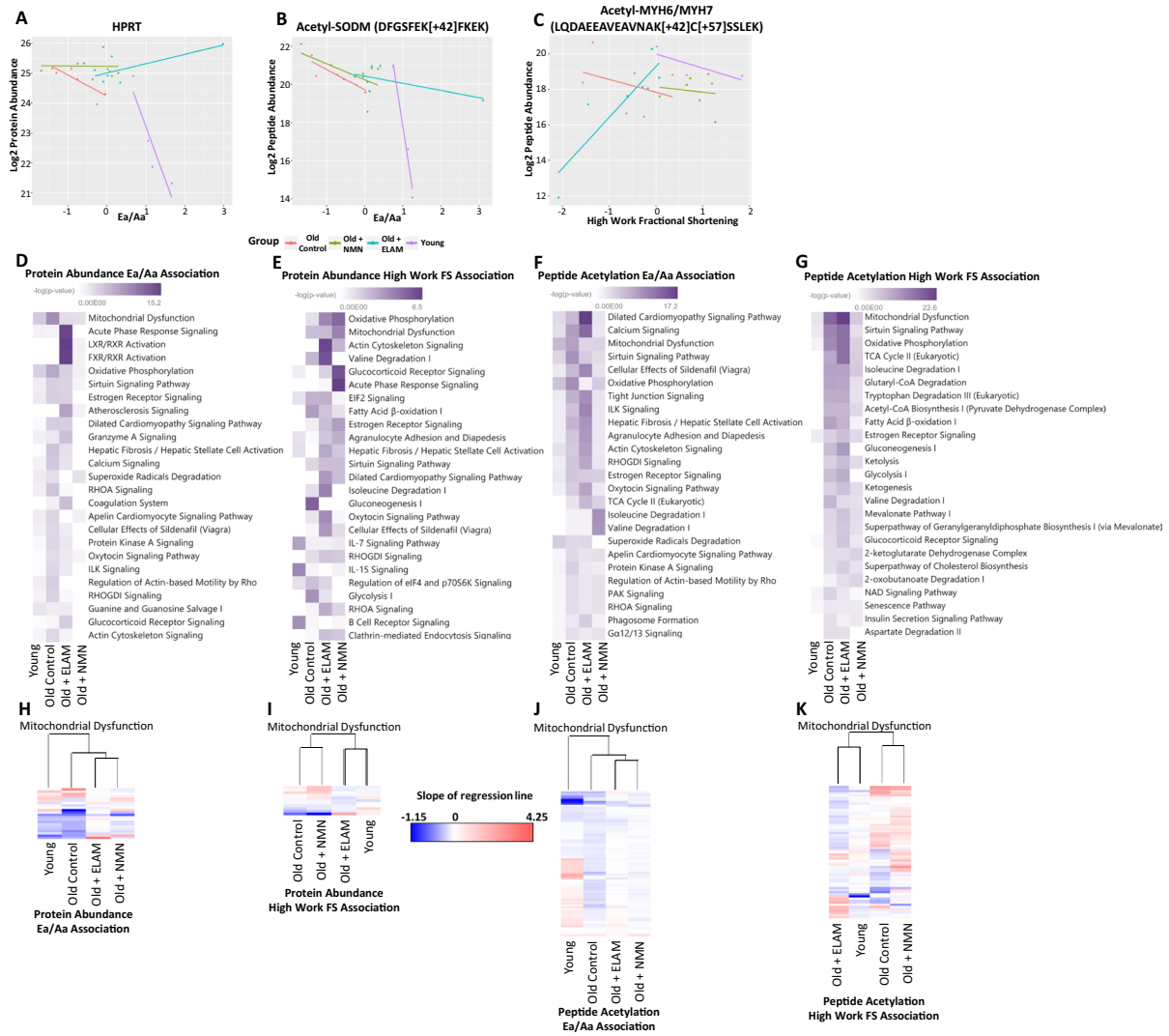

Fig. 3 Association of proteomic results with echocardiography measurements. **A**–**C** Examples of association analysis showing results for the association of **A** HPRT abundance with Ea/Aa, **B** acetyl-SODM (DFGSFEK[+42]FKEK) peptide with Ea/Aa, and **C** acetyl-MYH6/MYH7 (LQDAEEAVEAVNAK[+42]C[+57]SSLEK) peptide with high work fractional shortening. **D**–**G** *P*-value heatmaps of **D**, **E** protein abundance and **F**, **G** peptide acetylation association with heart functional changes in canonical pathways based on all associations with an unadjusted $P < 0.05$. Top 25 pathways, ranked by *P*-value, are shown. **H**–**K** Heatmaps of association of **H**, **I** protein abundance and **J**, **K** peptide acetylation with echocardiography measurements in mitochondrial dysfunction pathway. Heatmaps are not row normalized, with color representing the slope of the regression (darker blue, more negative association; darker red, more positive association)

diastolic function. Only two sites were associated with high work fractional shortening: a separate site on SODM, which showed a negative association in young hearts, and a site on a peptide mapping to myosin-6/7 (MYH6/7) which showed a positive association in old elamipretide-treated mouse hearts. The full set of peptide acetylation association results for all groups can be found in Appendix 2.

Further analysis of these association data was performed by IPA (QIAGEN) based on all proteins that had an association with an unadjusted $P < 0.05$ with the respective echocardiography measurement. This revealed an increased representation of many

Table 3 Significant Protein Abundance Association with Ea/Aa. Bold numbers indicate significance (FDR < 0.1). Ordered by lowest adjusted P-value across all comparisons. Full results can be found in Appendix 1

Protein	Slope of Association with Ea/Aa			
	Young	Old Control	Old ELAM	Old NMN
HPRT	**-3.57**	-0.70	0.31	-0.01
EGFR	0.24	0.24	**-1.49**	-0.12
FA10	-1.37	-1.12	**-1.18**	-0.36
A2AP	0.71	-0.43	**-0.76**	0.04
HEP2	0.96	-0.42	**-1.30**	0.17
TACC2	-0.56	-0.65	**0.58**	-0.10
RNF25	0.56	-0.14	**-1.15**	-0.34
PDK4	0.50	1.24	**1.32**	0.05
PALLD	-1.41	0.27	**-1.96**	-0.53
EST1C	0.03	-0.41	**-1.22**	-0.32
A1AT4	0.73	-0.49	**-0.91**	-0.34
MT2	-0.28	0.73	**1.02**	0.61
A1AT1	0.53	-0.18	**-0.75**	-0.25
LIFR	-0.59	0.19	**-2.12**	-0.97
HNRPK	-0.26	-0.14	**0.45**	0.06
AHNAK	-0.36	-0.51	**0.40**	-0.03
TNNT2	-0.71	0.05	**0.62**	-0.18
CPN2	0.11	-0.72	**-0.87**	-0.15
H2AX	-0.30	0.36	**0.50**	0.27
FETUB	0.19	0.03	**-0.51**	0.39
APOH	0.37	0.33	**-0.73**	-0.06
COF2	-0.18	0.22	**0.41**	-0.09
ICA	0.56	0.09	**-0.91**	-0.36
EST1	-0.08	-0.16	**-0.76**	-0.24
VTDB	-0.20	0.05	**-0.93**	0.07
SLIRP	0.14	-0.07	**-1.40**	-0.74
A1AT2	0.30	-0.08	**-0.65**	-0.15
Hbb-bs	0.51	0.39	**-0.58**	-0.27

pathways relating to mitochondrial health or cardiomyocyte function, including pathways of mitochondrial dysfunction, oxidative phosphorylation, calcium signaling, and dilated cardiomyopathy signaling, as expected (Fig. 3D–G). Interestingly, the TCA cycle showed a significant association with both Ea/Aa and high work fractional shortening in all old mouse groups when examined for acetylation, but not protein abundance.

Unscaled heatmaps of the association coefficients were generated for the mitochondrial dysfunction pathway (Fig. 3H–K), which was consistent among the most significantly overrepresented pathways in the analysis. For both protein abundance and peptide acetylation, old elamipretide- and NMN-treated hearts clustered more closely together with each other, and with old control hearts, than with young hearts when associating with Ea/Aa. When associating with high work fractional shortening, young and old + elamipretide hearts clustered closely together for both protein abundance and peptide acetylation.

Supplemental DATA

Supplemental data can be found at the end of the document. Full proteomic datasets can be found in the following appendices:

Appendix 1: Protein abundance analysis
Appendix 2: Peptide acetylation analysis

Raw data for protein abundance and peptide acetylation measurements are available on PanoramaWeb: https://panoramaweb.org/acetylLysMouseHeart.url (ProteomeXchange ID: PXD027458).

Discussion

How do elamipretide and NMN modulate the proteome?

Elamipretide and NMN had a limited effect on protein abundance at the individual level, although, when assessed as a whole, both drugs did appear to result in a slight restoration of pathways that showed decreased activation with age. The principal component analysis results also imply partial restoration of the proteome. Although these changes are subtle, we believe they are of functional consequence based on the association analysis. How NMN and elamipretide affect these changes is not yet entirely clear and likely results from a variety of factors, such as downstream signaling changes due to decreased oxidative stress, increased NAD^+-dependent enzyme activity, and improved mitochondrial health.

The overall trend in the acetylation data was that residues that were acetylated in young hearts lost much of this acetylation with age. However, there are exceptions where strong accumulation of acetylation with age was also seen along several pathways

Table 4 Significant Protein Acetylation Association with Ea/Aa. Bold numbers indicate significance (FDR < 0.1). Ordered by lowest adjusted P-value across all comparisons. Full results can be found in Appendix 2

Peptide	Maps to Proteins	Slope of Association with Ea/Aa			
		Young	Old Control	Old ELAM	Old NMN
DFGSFEK[+42]FKEK	sp|P09671|SODM_MOUSE	**-12.95**	-1.12	-0.39	-0.79
VVAGVAAALAHK[+42]YH	*tr|A8DUK4|A8DUK4_MOUSE|Hbb-bs*	2.46	-0.30	**-1.53**	-0.53
VAQLC[+57]DFNPK[+42]SSK	*sp|Q6IRU5|CLCB_MOUSE:sp|Q6IRU5-2|CLCB_MOUSE*	1.35	**-2.78**	0.42	-0.37
NLKPGEC[+57]LK[+42]VR	*sp|P16045|LEG1_MOUSE*	-0.37	**-4.14**	0.03	-0.49
K[+42]FLMEC[+57]R	*sp|Q60876|4EBP1_MOUSE*	0.99	**-3.92**	0.72	-0.71
HLNLSGNKIK[+42]	*sp|O35381|AN32A_MOUSE:sp|Q64G17|AN32C_MOUSE:tr|D3YYE1|D3YYE1_MOUSE:tr|D3Z7M9|D3Z7M9_MOUSE:tr|F6UFG6|F6UFG6_MOUSE*	2.30	**-3.63**	0.13	-0.18
LYVLK[+42]LYDK	*sp|Q9CR21|ACPM_MOUSE:tr|F6ZFT1|F6ZFT1_MOUSE:tr|F8WJ64|F8WJ64_MOUSE*	-11.91	**-5.91**	-2.13	-0.34
TC[+57]VAK[+42]GQAAVPR	*tr|A0A0G2JFH2|A0A0G2JFH2_MOUSE*	-0.26	**-2.67**	0.38	-0.44
LTMFGEK[+42]LK	*sp|P51667|MLRV_MOUSE:sp|Q62082|MYL10_MOUSE:tr|A0A0G2JDZ4|A0A0G2JDZ4_MOUSE:tr|A0A0G2JE15|A0A0G2JE15_MOUSE:tr|D3YUI7|D3YUI7_MOUSE:tr|D3YW14|D3YW14_MOUSE:tr|D3Z0I3|D3Z0I3_MOUSE:tr|E9Q8Y0|E9Q8Y0_MOUSE:tr|E9QNY3|E9QNY3_MOUSE:sp|Q62082-2|MYL10_MOUSE:sp|Q62082-3|MYL10_MOUSE:sp|P97457|MLRS_MOUSE:tr|A0A0U1RP93|A0A0U1RP93_MOUSE:tr|A0A0U1RQ36|A0A0U1RQ36_MOUSE*	0.92	**-1.76**	-0.03	-0.14
ISSPSGK[+42]IGAC[+57]R	*tr|E9Q616|E9Q616_MOUSE*	0.31	**-2.08**	0.66	-0.16
IDPEK[+42]LSVNSHFMK	*sp|Q9CR21|ACPM_MOUSE:tr|F6ZFT1|F6ZFT1_MOUSE:tr|F8WJ64|F8WJ64_MOUSE*	0.78	**-2.24**	0.04	-0.44
VASNLNLKPGEC[+57]LK[+42]VR	*sp|P16045|LEG1_MOUSE*	2.74	**-3.76**	0.19	-1.00
MMDFETFLPM[+16]LQHISKNK[+42]	*sp|P09542|MYL3_MOUSE:tr|A0A0G2JDM3|A0A0G2JDM3_MOUSE:tr|A0A0G2JDW2|A0A0G2JDW2_MOUSE*	3.07	**-3.28**	0.17	-0.82
TVFLTMFGEK[+42]LK	*sp|P51667|MLRV_MOUSE:sp|Q62082|MYL10_MOUSE:tr|A0A0G2JDZ4|A0A0G2JDZ4_MOUSE:tr|A0A0G2JE15|A0A0G2JE15_MOUSE:tr|D3YUI7|D3YUI7_MOUSE:tr|D3YW14|D3YW14_MOUSE:tr|D3Z0I3|D3Z0I3_MOUSE:tr|E9Q8Y0|E9Q8Y0_MOUSE:tr|E9QNY3|E9QNY3_MOUSE:sp|Q62082-2|MYL10_MOUSE:sp|Q62082-3|MYL10_MOUSE:sp|P97457|MLRS_MOUSE:tr|A0A0U1RP93|A0A0U1RP93_MOUSE:tr|A0A0U1RQ36|A0A0U1RQ36_MOUSE*	0.73	**-4.56**	-0.34	-0.74

and when looking at individual proteins. While loss of proper acetylation likely results from dysregulation of acetyltransferases with age, accumulation of acetylation with age implies potential deleterious non-enzymatic modification to proteins. Mitochondrial proteins are at particular risk for such spurious non-enzymatic acetylation due to the high levels of acetyl-CoA present [1].

One expected result of NMN treatment is a reduction of such hyperacetylation on mitochondrial

Table 5 Significant Protein Acetylation Association with high work fractional shortening in Old Control Hearts. Bold numbers indicate significance (FDR < 0.1). Ordered by lowest adjusted P-value across all comparisons. Full results can be found in Appendix 2

Peptide	Maps to Proteins	Slope of Association with High Work FS			
		Young	Old Control	Old ELAM	Old NMN
GGGEPKGELLEAIK[+42]R	*sp|P09671|SODM_MOUSE*	**-7.04**	0.06	1.33	-0.42
LQDAEEAVEAVNAK[+42]C[+57]SSLEK	*sp|Q02566|MYH6_MOUSE:sp|Q91Z83|MYH7_MOUSE*	-0.83	-0.58	**3.34**	-0.94

proteins through activation of sirtuins, attributed to an enhanced activity of the NAD^+-dependent mitochondrial deacetylases Sirt3 and Sirt5. Unfortunately, there is not a reliable way to test the specific activity of these two enzymes. This may be why our total sirtuin activity assay did not yield any significant results, including an inability to detect reduced sirtuin activity in Sirt3 knockout hearts. Thus, it is likely that mitochondrial sirtuins make up only a small part of the total sirtuin activity and cannot be properly assessed without first isolating mitochondria. The consistent identification of sirtuin signaling as a major pathway of significance in the protein abundance, peptide acetylation, and functional association results further points to the sirtuins as key regulators, although the interpretation of the biological significance of this in our study is not so straightforward. In particular, the inactivation of the sirtuin signaling pathway in young mice relative to old control in terms of protein abundance, but not by acetylation, is a surprising finding that has not previously been reported. This indicates that sirtuin substrates are significantly less abundant in young hearts but there does not appear to be detectable significant difference in the acetylation of these substrates overall, based on age. A more in-depth study of sirtuin activity in this context will need to be performed in the future to fully understand how these acetylation changes arise and what role the sirtuins play in heart aging and health.

Comparison to recent findings

Another recent study examined the effects of aging on the acetylation state of the heart proteome [20]. The report by Yeo et al. showed a significant increase in total acetylation with age in female mouse hearts by Western blot analysis whereas our proteomics data imply an overall trend of decreasing acetylation in the heart with age. To determine whether this discrepancy is due to a difference in methodology and/or mouse sex, we also assessed bulk acetylation of heart proteins by Western blot using an anti-acetyl-lysine antibody in male and female mice, although only male NMN-treated mice were available (Supplemental Fig. 3). Males did not show a significant increase in total acetylation of heart proteins with age while females actually displayed a significant decrease in total heart protein acetylation with age ($P < 0.05$). Treatment with elamipretide and NMN resulted in a significant ($P < 0.05$) increase in total acetylation in male mice while acetylation levels in elamipretide-treated females were midway between the young and old control and not significantly different from either. Thus, our Western blot data appear to support the conclusion from our proteomic analysis and both run counter to the Western blot data provided by Yeo et al. Comparing the blots from our analysis (Supplemental Figs. 4 and 5), with the blot of total heart acetylation from Yeo et al., our blots show many prominent bands across a range of molecular weights, consistent with the wide variety of proteins that can be acetylated, whereas the blot from Yeo et al. showed only two major bands. Therefore, these opposing results could be due to underexposure or differences in the antibody used by Yeo et al. In short, we did not observe any evidence of increased bulk acetylation in the heart, in males or females, with age. Our results also demonstrated that measuring bulk acetylation measurement is of lesser value, since it is the activation and inactivation of specific proteins and pathways that ultimately affects function.

Yeo et al. also reported an age-related increase in NAMPT levels, which is in agreement with our protein abundance data that also showed significantly increased NAMPT levels with age (Appendix 1). Thus, our data from this study and our previous work

[18] appear to be in agreement with Yeo et al. and other reports [8] that the decline in NAD^+ levels with age is not due to a decrease in the salvage pathway of NAD^+ but rather can be attributed to greater NAD^+ utilization by enzymes.

Association of proteins and acetylation sites with heart function identifies mediators of cardiac dysfunction

By correlating the age-related protein abundance and acetylation changes that occur in individual mouse hearts with how functional parameters change in those same hearts, we have been able to provide new insights into the mechanism by which proteomic modifications may play a role in cardiac aging. Some of these proteins, such as myosin chains and cytoskeletal components, already have a known role in cardiac function. Others, like SODM, do not have well-defined roles in the heart. Such proteins present promising new targets for the further investigation of heart health and mechanisms of cardiac aging.

Interestingly, with the exception of HPRT in young mice, all of the significant (FDR < 0.1) associations of protein abundances with Ea/Aa were in the old elamipretide-treated group. Because elamipretide treatment enhances Ea/Aa in old hearts [2, 18], it can be presumed that changes in the abundance of the noted proteins are at least partially responsible for this recovery in diastolic function. Conversely, as no associations between protein abundance and high work fractional shortening were significant, the data indicate that changes to protein abundance are not a major regulatory mechanism of systolic function in aging. This fits well with our prior assertion that metabolic changes account instead for much of the functional difference in systolic function with age and drug treatment [18].

Although the general trend in our acetylation data was that acetylation is lost with age, the association analysis revealed many sites where acetylation had a negative association with Ea/Aa in old control mice. This indicates that, along this set of proteins, greater acetylation is associated with decreased diastolic function. As many of these sites are located on muscle and mitochondrial proteins, we believe these results are indicative of the accumulation of age-related nonenzymatic hyperacetylation that accounts for the loss of function, along with other PTMs [19]. However, there was also a strong association between increased acetylation of a site on MYH6/7 and high work fractional shortening in old elamipretide-treated hearts, showing that enhanced acetylation of essential cardiac proteins may be beneficial for systolic function in some limited circumstances.

Limitations

While these data provide compelling mechanistic insights for targeting cardiolipin (elamipretide) or the NAD^+/NADH pool (NMN) in aged mice, the dose of NMN administered to mice in the study is roughly 50 times higher than available dietary NMN supplements. Future studies to better understand the dose dependency of these findings will advance our understanding of these treatments in mitigating age-related cardiac changes.

We were also unable to determine for how long and to what degree the proteomic changes we have noted that result from these drug treatments persist after treatment is ceased. Our previous studies demonstrated that the functional effects induced in old hearts from elamipretide and NMN treatment persist for several weeks and days, respectively, following the end of treatment [2, 18]. Thus, we expect that the proteomic changes, which are associated with functional changes, would follow a similar timeline.

Lastly, we could not include a group of mice treated simultaneously with elamipretide and NMN in this study due to sample limitations. We acknowledge that the drugs given in combination may result in additional proteomic changes not observed when each is given in isolation.

Conclusions

In total, these results greatly expand our understanding of how changes in protein abundance and acetylation play a role in the functional changes that occur in the heart due to age and treatment with elamipretide and NMN. By associating specific proteomic changes with alterations in diastolic and systolic function, we identified new targets for the treatment of age-related heart disease that warrant additional study. Furthermore, the data we have provided enhances our understanding of the differential effects induced by elamipretide and NMN, which helps to explain the

previously reported synergistic effect of administering both drugs simultaneously [18].

Experimental procedures

Animal use and care

All mice used were of the C57BL/6 strain. Male mice were used for all measurements with the exception of Western blot, which also included females. Young and old mice were obtained from the National Institute on Aging Charles River colony and further aged to 5–6 and 24 months, respectively, before starting the study. Mice were kept under diurnal conditions with ad libitum food and water. Mice were housed at 20 °C under diurnal conditions in an AAALAC accredited facility under Institutional Animal Care Committee supervision with ad libitum access to food and water. Old mice were randomly assigned to control, elamipretide, NMN, or combined treatment groups.

Drug administration and treatment groups

Elamipretide was provided by Stealth BioTherapeutics (Needham, MA). In accordance with previous studies demonstrating its effectiveness [2, 15, 18, 19], elamipretide was administered at a 3 mg/kg body weight/day dosage through osmotic minipumps (ALZET, Cupertino, CA) implanted surgically under the skin on the left dorsal side of the mice. This route of administration was used since, as a peptide, elamipretide is not orally bioavailable and osmotic minipump placement results in a more even dosage and less stress to the mice compared to repeated twice daily intraperitoneal injections. After 4 weeks, the original minipump was surgically removed and a new minipump was implanted to continue the elamipretide administration for another 4 weeks.

NMN was obtained from the Imai Lab (Washington University in St. Louis, MO) and administered through ad libitum drinking water with a concentration based on each cage's measured water consumption rate and mean body weight. Mice ingested approximately 300 mg/kg body weight/day NMN, which was previously demonstrated to be an effective dose to increase tissue NAD^+ levels and alter various physiological functions in these animals [9]. NMN water was the only source of hydration given to these mice and was replaced every 3–7 days based upon prior tests showing that it remains stable under these conditions for at least 1 week [9].

Euthanasia and tissue handling

At the conclusion of the experiment, mouse numbers were 8 young, 8 old control, 8 old elamipretide, and 7 old NMN. Mice were euthanized by live cervical dislocation. Hearts were immediately removed, rinsed with PBS, and weighed. A 2 mm section was removed from the ventricles for histology and the remaining tissue was cut into ~ 2 mm^3 chunks and snap frozen in liquid N_2 to store for further processing. Frozen tissue was mechanically lysed into a fine powder using a TissueLyser II (QIAGEN) prior to mass spectroscopy.

Unmodified peptide proteomics

Powdered heart tissue was homogenized by probe sonication in ice-cold extraction buffer (0.1% RapiGest surfactant in 100 mM Tris–HCl pH 8.0) with 10 µM trichostatin A and 10 mM nicotinamide in order to preserve the acetylation state of proteins. Protein was digested using trypsin and samples were spun down at 12,000 × g to remove insoluble materials. Peptides were purified using MCX columns following the manufacturer's instructions (Waters). Samples were dried using a CentriVap Concentrator (LABCONCO, Kansas City, MO) and reconstituted in 0.1% formic acid with 16.67 fmol/µl PRTC. Samples were diluted and solubilized in 180 µl of HPLC loading buffer (0.1% trifluoracetic acid and 2% acetonitrile) by vortexing for 10 min at 37 °C to give an estimated final concentration of 0.11 µg/µl. The solubilized samples were centrifuged at 10,000 × g for 5 min to pellet any particulates that might cause HPLC clogging, and then a portion of each supernatant was placed into autosampler vials. Injection volumes were 3 µl. Samples were run in blocks containing single replicates of each condition, where the order within each block was randomized.

All mass spectrometry was performed on a Q Exactive HF-X (Thermo Fisher Scientific, Waltham, MA). Samples were loaded from the autosampler onto a 150-µm Kasil fritted trap packed with ReproSil-Pur 120 Å C18-AQ 3 µm beads (Dr. Maisch High Performance LC, Ammerbuch-Entringen, Germany) to a bed length of 2 cm at a flow rate of 2 µl/min

for 4 min. After loading and desalting, the trap was brought in-line with a pulled fused-silica capillary tip (75-µm ID) packed with 30 cm of the same chromatography material mounted in a nanospray source with the column and trap heated to 50 °C. Peptides were eluted off the trap and column using a Thermo Easy-nLC 1200 HPLC using flow rate of 250 nl/min and a gradient of 0–32% acetonitrile in 0.1% formic acid over 90 min, followed by 32–60% gradient over 5 min, and a subsequent column wash at 80% acetonitrile.

The mass spectrometer was operated using electrospray ionization (2 kV) with the heated transfer tube at 275 °C in data-independent acquisition (DIA) mode covering a precursor range of *m*/*z* 400 to 1000. The quadrupole isolation width was set to *m*/*z* 8, MS/MS resolution was 15,000 at *m*/*z* 200, the automatic gain control target was set to 1e6, and the maximum fill time was set to 22 ms. For every other cycle of DIA covering the entire precursor range, the isolation windows were offset by *m*/*z* 4 in order to obtain overlapping DIA windows that could be deconvolved, resulting in an effective isolation width of *m*/*z* 4. The normalized collision energy was set at 28% with a default charge state of 2. Each cycle of DIA was preceded by an MS acquisition from *m*/*z* 400 to 1000 at a resolution of 30,000 with an AGC target of 3e6 covering *m*/*z* 400–1000. Chromatogram libraries were made from the two pooled samples (pre- and post-enrichment) in a similar manner except that the quadrupole isolation width was *m*/*z* 4 with alternating overlap to give an effective isolation width of *m*/*z* 2. Data-dependent acquisition (DDA) data was also acquired on the two pools using resolution of 60,000 in MS1 with 3e6 as the AGC target. For MS2, the quadrupole isolation width was set to 1.6, the resolution 15,000, the AGC target 22 ms, and gas phase fractionation was used covering the precursor ranges of *m*/*z* 400–600, 600–900, and 900–1600.

Data analysis first required demultiplexing the overlapping DIA data using MSconvert (Proteowizard v3.0.19268) to convert the Thermo raw files to mzML files. The vendor centroid option was chosen, along with the demultiplex filter using "overlap only" with a mass error of 10 ppm. A spectral library was created from the pooled pre-enrichment DDA data that was used by Encyclopedia v0.9 and the *m*/*z* 4 overlapping DIA data to make a chromatogram library containing precisely determined retention times. This chromatogram library was used to analyze the DIA data for the individual samples (*m*/*z* 8 isolation with overlapping windows). The same was done for the post-enrichment samples, except that the initial DDA library was comprised of our own data obtained from a pooled sample, plus DDA data obtained from the laboratory of James Bruce [6].

Peptide intensity values were normalized by sample total ion current (TIC) and rolled up to generate protein abundance values using Encyclopedia software by parsimonious protein detection [14]. Statistical analysis and further normalization were performed using R scripts. Missing values in this analysis are also believed to be MNAR in nature. We chose the quantile regression approach for the imputation of left-censored missing data (QRILC), which has been suggested as the favored imputation method for left-censored MNAR data [17]. Briefly, QRILC performs the feature-level imputation by replacing missing values with random draws from a truncated distribution with parameters estimated using quantile regression. This is implemented in the R imputeLCMD package. In order to remove any unwanted variation in the data, we used the Bioconductor SVA package to identify and estimate surrogate variables (SVs) [7]. The estimated SVs are included in the model as covariates for the subsequent analyses. We fit a linear model to the protein level data to detect the group differences using the Bioconductor limma package [12], while controlling for the estimated SVs as covariates in our model. False discovery rate (FDR) was limited to 10% using the Benjamini–Hochberg method.

Acetylated peptide analysis

From the DIA proteomics preparation described above, 700 µg of peptides from each sample was taken prior to drying and subjected to a pulldown for the enrichment of acetylated peptides using the Acetyl-Lysine PTMScan Kit following the manufacturer's instructions (Cell Signaling Technologies, Danvers, MA). Following this pulldown, peptides were run under the same conditions described for standard DIA proteomics as described above, with the following changes. The acetyl-lysine-enriched samples were diluted and solubilized in 30 µl of loading buffer. Injection volumes were 15 µl for the enriched samples. In all cases, the enriched sample was run immediately after its matching unenriched sample.

Following data acquisition, only peptides containing at least one lysine residue with a + 42 molecular weight modification were analyzed. Since the total number of acetylated peptides in the eluent may vary between the different treatments based on the amount of acetylation present, the acetyl-enriched results were normalized by the TIC of the unenriched DIA sample runs (i.e., normalized by the material input into the pulldown) rather than the TIC of the enriched fraction. Further normalization and statistical analysis were performed as described above for DIA abundance proteomics.

Sirtuin activity assay

The Fluorometric Sirtuin Activity Assay Kit (EPI018) was used to assess bulk sirtuin activity in heart samples following the manufacturer's instructions (MilliporeSigma, St. Louis, MO).

Echocardiography

Echocardiography was performed as described previously [18]. Briefly, mice were anesthetized by 0.75–2% isoflurane and echocardiography was performed using a Siemens Acuson CV-70 (Munich, Germany) equipped with a 13 MHz probe. High work rate was induced by injection of 3 μg/g body weight dobutamine.

Association analysis

Ea/Aa and high work fractional shortening measurements were first standardized to have a mean of 0 and standard deviation of 1. We fit a linear model to the protein abundance and acetylation data to detect if there is a linear relationship between these protein or acetylated peptide measurements and the standardized Ea/Aa or the standardized high work fractional shortening measurements obtained from echocardiography in the same mice within each group. This is implemented in the Bioconductor limma package [12], while controlling for the estimated SV as a covariate in our model. We used Benjamini–Hochberg method for multiple testing correction procedure and selected proteins or acetylated peptide with a FDR of 10%.

Western blotting

Proteins were extracted from frozen heart tissues homogenized with a 5 mm stainless steel bead in a QIAGEN TissueLyser. Powder was resuspended in RIPA buffer with protease and phosphatase inhibitors and quantified by BCA protein assay (Thermo Fisher Scientific #23,225). Ten micrograms of protein was resolved on 4–12% NuPAGE Bis–Tris gel (Thermo Fisher Scientific #WG1403BOX) and transferred to PVDF membrane. A Pierce Reversible Protein Stain Kit (Thermo Fisher Scientific #24,585) was used to detect total proteins for normalization of loading.

The primary antibody used in immunoblotting was acetylated lysine (Cell Signaling Technology #9441S). Secondary antibody used was donkey anti-rabbit IgG secondary antibody (Thermo Fisher Scientific #A16035). SuperSignal West Dura Chemiluminescent Substrate (Thermo Fisher Scientific #34,076) was used for detection and AlphaView software (ProteinSimple/Bio-Techne, San Jose, CA) was used for image acquisition and quantification.

Statistical analysis

Statistical analyses of large-scale proteomics data are described in the above sections. All other data were analyzed by one- or two-way ANOVAs, as appropriate, with correction for multiple comparisons using Prism software (GraphPad Software, San Diego, CA). All results are plotted as means ± SEM.

Funding Funding for this research was provided by NIH grants T32AG000057, P01AG001751, the UW Nathan Shock Center, P30 AG013280, and AHA 19CDA34660311. Elamipretide was kindly provided by Stealth Therapeutics (Needham, MA). Stealth BioTherapeutics did not play any role in the experimental design, data collection, or authorship of this work. The laboratory of James Bruce kindly provided DDA data on heart peptide acetylation for the purposes of building a peptide library [6].

Declarations

Conflict of interest The authors declare no competing interests.

References

1. Baeza J, Smallegan MJ, Denu JM. Site-specific reactivity of nonenzymatic lysine acetylation. ACS Chem Biol. 2015;10(1):122–8. https://doi.org/10.1021/cb500848p.
2. Chiao YA, Zhang H, Sweetwyne M, Whitson J, Ting YS, Basisty N, Pino LK, Quarles E, Nguyen NH, Campbell MD, Zhang T, Gaffrey MJ, Merrihew G, Wang L, Yue Y, Duan D, Granzier HL, Szeto HH, Qian WJ, … Rabinovitch P. Late-life restoration of mitochondrial function reverses cardiac dysfunction in old mice. Elife. 2020;9:1–26. https://doi.org/10.7554/eLife.55513.
3. Dai D-F, Chen T, Johnson SC, Szeto H, Rabinovitch PS. Cardiac aging: from molecular mechanisms to significance in human health and disease. Antioxid Redox Signal. 2012;16(12):1492–526. https://doi.org/10.1089/ars.2011.4179.
4. Grant JE, Bradshaw AD, Schwacke JH, Baicu CF, Zile MR, Schey KL. Quantification of protein expression changes in the aging left ventricle of Rattus norvegicus. J Proteome Res. 2009;8(9):4252–63. https://doi.org/10.1021/pr900297f.
5. Krämer A, Green J, Pollard J, Tugendreich S. Causal analysis approaches in Ingenuity Pathway Analysis. Bioinformatics. 2014;30(4):523. https://doi.org/10.1093/BIOINFORMATICS/BTT703.
6. Lee CF, Chavez JD, Garcia-Menendez L, Choi Y, Roe ND, Chiao YA, Edgar JS, Goo YA, Goodlett DR, Bruce JE, Tian R. Normalization of NAD+ redox balance as a therapy for heart failure. Circulation. 2016;134(12):883–94. https://doi.org/10.1161/CIRCULATIONAHA.116.022495.
7. Leek JT, Storey JD. Capturing heterogeneity in gene expression studies by surrogate variable analysis. PLoS Genet. 2007;3(9):1724–35. https://doi.org/10.1371/journal.pgen.0030161.
8. Liu L, Su X, Quinn WJ, Hui S, Krukenberg K, Frederick DW, Redpath P, Zhan L, Chellappa K, White E, Migaud M, Mitchison TJ, Baur JA, Rabinowitz JD. Quantitative analysis of NAD synthesis-breakdown fluxes. Cell Metab. 2018;27(5):1067-1080.e5. https://doi.org/10.1016/j.cmet.2018.03.018.
9. Mills KF, Yoshida S, Stein LR, Grozio A, Kubota S, Sasaki Y, Redpath P, Migaud ME, Apte RS, Uchida K, Yoshino J, Imai S. Long-term administration of nicotinamide mononucleotide mitigates age-associated physiological decline in mice. Cell Metab. 2016;24(6):795–806. https://doi.org/10.1016/j.cmet.2016.09.013.
10. Morimoto RI, Cuervo AM. Proteostasis and the aging proteome in health and disease. J Gerontol A Biol Sci Med Sci. 2014;69(Suppl 1):S33-8. https://doi.org/10.1093/gerona/glu049.
11. Quarles E, Basisty N, Chiao YA, Merrihew G, Gu H, Sweetwyne MT, Fredrickson J, Nguyen NH, Razumova M, Kooiker K, Moussavi-Harami F, Regnier M, Quarles C, MacCoss M, Rabinovitch PS. Rapamycin persistently improves cardiac function in aged, male and female mice, even following cessation of treatment. Aging Cell. 2020;19(2). https://doi.org/10.1111/acel.13086.
12. Ritchie ME, Phipson B, Wu D, Hu Y, Law CW, Shi W, Smyth GK. Limma powers differential expression analyses for RNA-sequencing and microarray studies. Nucleic Acids Res. 2015;43(7): e47. https://doi.org/10.1093/nar/gkv007.
13. Santos AL, Lindner AB. Protein posttranslational modifications: roles in aging and age-related disease. Oxid Med Cell Longev. 2017;2017:5716409. https://doi.org/10.1155/2017/5716409.
14. Searle BC, Pino LK, Egertson JD, Ting YS, Lawrence RT, MacLean BX, Villén J, MacCoss MJ. Chromatogram libraries improve peptide detection and quantification by data independent acquisition mass spectrometry. Nat Commun. 2018;9(1). https://doi.org/10.1038/s41467-018-07454-w.
15. Thomas DA, Stauffer C, Zhao K, Yang H, Sharma VK, Szeto HH, Suthanthiran M. Mitochondrial targeting with antioxidant peptide SS-31 prevents mitochondrial depolarization, reduces islet cell apoptosis, increases islet cell yield, and improves posttransplantation function. J Am Soc Nephrol. 2007;18(1):213–22. https://doi.org/10.1681/ASN.2006080825.
16. Walther DM, Kasturi P, Mann M, Ulrich F, Correspondence H. Widespread proteome remodeling and aggregation in aging C. elegans. 2015. https://doi.org/10.1016/j.cell.2015.03.032.
17. Wei R, Wang J, Su M, Jia E, Chen S, Chen T, Ni Y. Missing value imputation approach for mass spectrometry-based metabolomics data. Sci Rep. 2018;8(1). https://doi.org/10.1038/s41598-017-19120-0.
18. Whitson JA, Bitto A, Zhang H, Sweetwyne MT, Coig R, Bhayana S, Shankland EG, Wang L, Bammler TK, Mills KF, Imai S, Conley KE, Marcinek DJ, Rabinovitch PS. SS-31 and NMN: two paths to improve metabolism and function in aged hearts. Aging Cell. 2020. https://doi.org/10.1111/acel.13213.
19. Whitson JA, Martín-Pérez M, Zhang T, Gaffrey MJ, Merrihew GE, Huang E, White CC, Kavanagh TJ, Qian W-J, Campbell MD, MacCoss MJ, Marcinek DJ, Villén J, Rabinovitch PS. Elamipretide (SS-31) treatment attenuates age-associated post-translational modifications of heart proteins. GeroScience. 2021. https://doi.org/10.1007/s11357-021-00447-6.
20. Yeo D, Kang C, Ji LL. Aging alters acetylation status in skeletal and cardiac muscles. GeroScience. 2020;42(3):963–76. https://doi.org/10.1007/s11357-020-00171-7.